Nonlinear Spline Generation with Curve Evolutions Driven by Curvature

Alexander G. Belyaev belyaev@u-aizu.ac.jp
Elena V. Anoshkina c98elena@u-aizu.ac.jp
Shin Yoshizawa s1031157@u-aizu.ac.jp

The University of Aizu, Aizu-Wakamatsu City, Fukushima 965-8580, Japan

Abstract

The paper develops a method to design nonlinear splines on a plane via curve evolutions driven by curvature. We consider a curve passing through two given end-points and satisfying prescribed boundary conditions at them (for example, curvature values or tangent directions are specified at the end-points). Each point of the curve moves in the normal direction with speed equal to a function of the curvature and curvature derivatives at the point. Chosen the speed function properly, the evolving curve converges to a desired nonlinear spline.

We also consider evolutions of closed curves for purposes of multiscale shape analysis.

Smooth curve evolutions are approximated by evolutions of polygonal curves. Discrete analogs of the curvature and its derivatives are considered.

Introduction

Let us consider a family of smooth curves $\mathcal{C}(p,t)$, where p parameterizes the curve and t parameterizes the family, either connected two given end-points or closed. We suppose p to be independent of t.

Let us assume that this family evolves according to the evolution equation

$$\frac{\partial \mathcal{C}(p,t)}{\partial t} = F\,\mathbf{n}, \qquad \mathcal{C}(p,0) = \mathcal{C}^{(0)}(p), \tag{1}$$

where $\mathbf{n}(p,t)$ is the unit normal vector for $\mathcal{C}(p,t)$, F is a speed function. The family parameter t can be considered as the time duration of the evolution.

The speed functions F in (1) may depend on many factors including local and global properties of the evolving curve, time t, and properties independent of the evolving curve.

The study of families of plane curves evolving according to (1) has recently been the subject of much research. Besides the mathematical beauty of such curve evolutions they have been studied in connection with multiscale shape analysis [9, 16], geometrical image processing (active contours) and computer vision [6, 12, 13, 17] (see also references therein and a recent review on active contour models in [19]). Evolutions of polygons for shape analysis purposes were considered in [2, 3].

In the present paper we apply curve evolution (1) to model nonlinear splines.

Throughout the paper, s will stand for arc length and a prime $'$ will mean the derivative with respect to arc length.

The main idea

Suppose we want to join two given points on a plane by a smooth curve along which

$$F \equiv 0. \tag{2}$$

The idea is to consider evolution (1) of a family of smooth curves passing through the endpoints. Let the evolving curve converge to a limit curve $\mathcal{C}^{(\infty)}$:

$$\mathcal{C}(p,t) \longrightarrow \mathcal{C}^{(\infty)}(p) \quad \text{as} \quad t \to \infty. \tag{3}$$

Since the evolution does not change the limit curve $\mathcal{C}^{(\infty)}$, then $F \equiv 0$ along $\mathcal{C}^{(\infty)}$.

Often nonlinear splines can be defined as curves minimizing energy functionals and we choose spline generating evolutions closely related to the gradient descent flows of such energy functionals.

Let us consider several examples where this approach can be used.

- Consider a plane domain equipped with the conformal metric $dl^2 = g(x,y)^2\,ds^2$, where $ds^2 = dx^2 + dy^2$ is the standard Euclidean metric. The *geodesics* are curves minimize locally the integral (length functional)

$$\int dl = \int g(x,y)\,ds.$$

The gradient descent flow is given by (1) with

$$F = gk - \nabla g \cdot \mathbf{n}, \tag{4}$$

where k is the curvature. See Appendix A for details. The quantity $gk - \nabla g \cdot \mathbf{n}$ is called the geodesic curvature associated with the metric dl^2.

- The *elastica* curves minimize the integral

$$\int \left(C_1 \frac{k^2}{2} + C_2 \right) ds,$$

where k is the curvature and s is arc length. Here C_1 and C_2 are positive constants. The gradient descent flow is given by (1) with

$$F = -C_1 \left(k'' + \frac{k^3}{2} \right) + C_2\, k$$

(see, for example, [12]). Elastica curves are used in computer vision to reconstruct hidden contours [6, 12].

- The *mechanical splines* [7] are a particular case of the elastica curves. The mechanical splines minimize the energy

$$\frac{1}{2} \int k^2\, ds$$

and are characterized by the equation

$$k'' + \frac{1}{2} k^3 = 0. \tag{5}$$

The gradient descent flow is defined by (1) with

$$F = -k'' - \frac{1}{2} k^3. \tag{6}$$

Derivation is given in Appendix A.

- A *wooden spline* [7] is characterized by the equation

$$k'' = 0,$$

that means the curvature varies linearly along the spline

$$k(s) = c_1 + c_2 s,$$

where c_1 and c_2 are constants. It defines a curve called a *Cornu spiral*, *Euler spiral*, or *clothoid*. A variational principle for the wooden splines can be found in [18]. The gradient descent flow is given by (1) with

$$F = -k''. \tag{7}$$

- A variety of other nonlinear splines defined via variational principles can be found in [11, 1] (see also references therein).

Numerical implementation

There are several strategies to solve (1) numerically. Among them we would like to mention

– marker/string methods;

– volume-of-fluid techniques;

– level set methods.

A review of numerical techniques for tracking interfaces can be found in [17]. The marker/string methods are more accurate numerically but have difficulties to handle topological changes of moving interfaces to compare with the volume-of-fluid and level set methods. Since our primal goal is to evolve curves with speed depending on high-order curve derivatives (the second-order derivative of the curvature of a curve involves the fourth-order derivatives of the curve), we prefer to use a marker/string method.

To solve (1) numerically we first replace the time derivative term by its forward difference approximation

$$\frac{\partial \mathcal{C}(p,t)}{\partial t} \approx \frac{\mathcal{C}(p,t+\varepsilon) - \mathcal{C}(p,t)}{\varepsilon}, \qquad \varepsilon \ll 1.$$

It gives

$$\mathcal{C}(p,t+\varepsilon) = \mathcal{C}(p,t) + \varepsilon\, F\, \mathbf{n}.$$

We approximate smooth curves by polygonal lines for which we introduce discrete analogs of the curvature, tangent and normal vectors. For a polygonal curve given by its vertices $\{P_i\}_{i=1}^{M}$ we consider discrete evolution shifting each vertex according to

$$P_i^{(k+1)} = P_i^{(k)} + \varepsilon^{(k)}\, F_i^{(k)}\, \mathbf{n}_i^{(k)}. \tag{8}$$

Here $P_i^{(k)}$ indicates the location of vertex i after k iterations, $\mathbf{n}_i^{(k)}$ is the unit normal vector at $P_i^{(k)}$, $F_i^{(k)}$ and $G_i^{(k)}$ is a discrete approximation of the function F, the iterative step parameter $\varepsilon^{(k)}$ is sufficiently small. See Fig. 1.

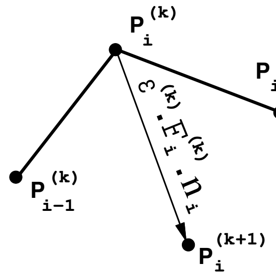

Figure 1.

We choose $\varepsilon^{(k)}$ depending on $d_{\min}^{(k)}$, the length of the minimal link of the polygonal curve $\{P_i^{(k)}\}$. For example, for evolution (1) with speeds (6) and (7) we set

$$\varepsilon^{(k)} = \varepsilon_0 \left[d_{\min}^{(k)} \right]^3$$

in order to make the evolution scale invariant.

If (3) is valid we can expect the convergence

$$\{P_i^{(k)}\} \longrightarrow \{P_i^{(\infty)}\}$$

We terminate discrete evolution (8) at the step N if $\max_i |F_i^{(N)}|$ or another norm of the vector $\{F_i^{(N)}\}$ is sufficiently small.

Discrete approximations of curvature, curvature derivatives, and normal direction

Circle approximation of curvature. Let us use the circle passing through the points A, O, B as an approximation to the osculating circle to the curve at O, see Fig. 2. Then the

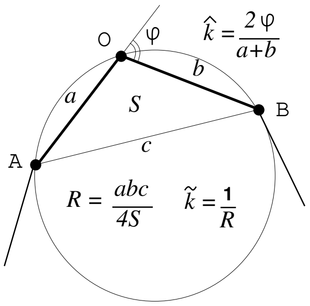

Figure 2.

inverse value of the radius will serve as an approximation of the curvature at O. This curvature approximation was considered in [11]. Let S denote the area of the triangle AOB. The discrete curvature at O is given by

$$\widetilde{k} = \frac{4S}{abc}. \tag{9}$$

Angle approximation of curvature. Another idea to define the curvature of a polygonal line is based on the definition of the curvature as the rate of change of the angle between the tangent and the positive direction of the x-axis when we proceed along the curve. Let φ denote the turn angle at O (see Fig. 2). Following [1, 13] let us define the discrete curvature at O as

$$\widehat{k} = \frac{2\varphi}{a+b}. \tag{10}$$

For the curve evolutions involving the second derivative of the curvature in addition to fixed end points we need to specify either curvature values or tangents at the end points. If curvature values are prescribed, it is better to use approximation (9). If tangents are specified, it is better to use approximation (10).

Discrete approximations of curvature derivatives. We estimate the first and second derivatives of the curvature at O by symmetric quotients

$$k'(O) \approx \frac{k(B)-k(O)}{b} + \frac{k(O)-k(A)}{a} - \frac{k(B)-k(A)}{a+b},$$
$$k''(O) \approx \frac{2k(A)}{a(a+b)} - \frac{2k(O)}{ab} + \frac{2k(B)}{b(a+b)}.$$

Discrete approximations of normal. At any vertex of a polygonal curve (except, of course, end-points, if the tangents at them are prescribed) we define the tangent direction as the direction orthogonal to a normal direction.

For a polygonal curve given by its vertices $\{P_i\}_{i=1}^{M}$ let us define a normal direction at P_i as the **bisector direction** of the angle $\angle P_{i-1}P_iP_{i+1}$, see the left image of Fig. 3. For

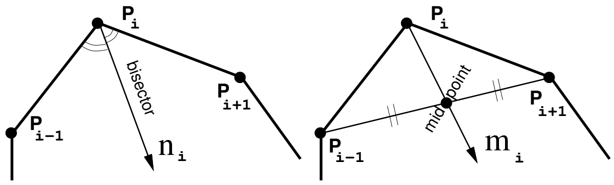

Figure 3.

an oriented polygonal line we denote by $\mathbf{n}_i$ the unit normal vector associated with the bisector direction at vertex P_i.

However using the bisector direction as the normal leads to developing irregularities in the distribution of the vertices along the polygonal curve even for the simplest curve shortening evolution

$$\frac{\partial \mathcal{C}(p,t)}{\partial t} = k\,\mathbf{n}. \tag{11}$$

A possible remedy lies in another definition of the normal direction for a polygonal curve. Let us define the normal direction at P_i as the direction of the line passing through P_i and the midpoint of the segment $P_{i-1}P_{i+1}$, the **median direction**, see the right image of Fig. 3. For an oriented polygonal line we denote by $\mathbf{m}_i$ the unit normal vector associated with the median direction at vertex P_i.

Numerical experiments

The median direction definition of the normal works perfectly for the evolutions (1) with the speed F depending on the curvature only: $F = F(k)$. For example, Fig. 4 demonstrates polygons (after a proper rescaling) obtained during the evolution of a initial polygon under the discrete flow

$$P_i^{(n+1)} = P_i^{(n)} + \varepsilon^{(n)}\, k_i^{(n)}\, \mathbf{m}_i^{(n)} \qquad (12)$$

associated with (11). Here $k_i^{(n)}$ is the discrete curvature at $P_i^{(n)}$ and $\mathbf{m}_i^{(n)}$ is the unit median vector at $P_i^{(n)}$. Our

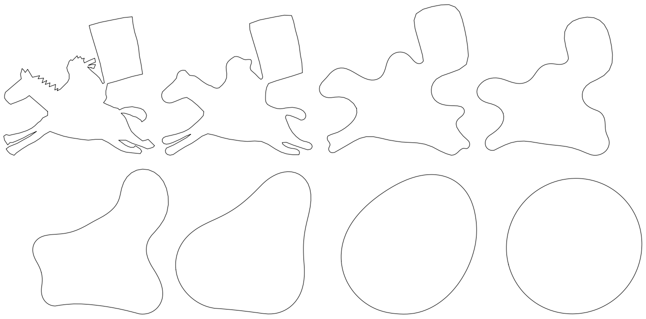

Figure 4. From left to right, from top to bottom: evolution of a closed polygon with speed equal to curvature.

experiments with polygons deformed by (12) show that

- the flow first reduces small, narrow, and edgy protrusions;
- a nonconvex polygon becomes convex and then it tends to a regular polygon and simultaneously shrinks into a point;
- for any interval of time, if the step-size parameter ε is small enough no new curvature extrema are generated.

Fig. 5 shows generation of a polygonal approximation of a geodesic on the *Lobachevsky plane* (the upper half plane $\{(x, y),\, y > 0\}$ equipped with the metric $(dx^2 + dy^2)/y^2$).

A discrete analog of (1), (4) modifies an initial polygonal line into a polygonal line approximated an arc of a circle centered on the x-axis (the geodesics on the Lobachevsky plane are the semicircles centered on the x-axis and vertical half lines).

Surprisingly, the discrete evolutions with the normal vector defined via the median direction are unstable when the speed F depends on the second derivative of the curvature k''. To tackle such cases we use the unit normal $\mathbf{n}$ defined via the bisector direction. Fig. 6 demonstrates the evolution of an initial polygonal line under a discrete analog of the flow (1), (7). To avoid instabilities evoked by nonuniform distribution of vertices along the evolving polygonal line we need to choose the step-size parameter ε very small and the evolution converges slowly.

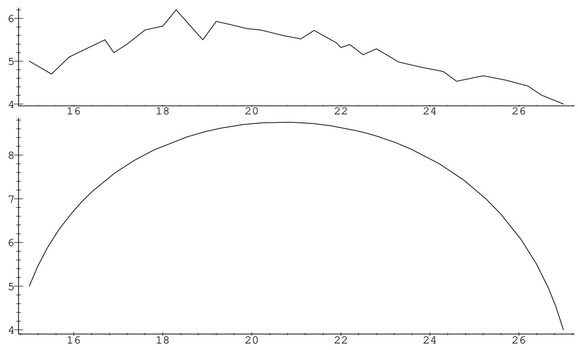

Figure 5. Modeling of a geodesic on the Lobachevsky plane. Top: An initial curve. Bottom: A geodesic obtained as the limit curve.

In general, for evolving polygonal lines with equal-length links we can choose the step-size parameter ε bigger then for evolving polygonal lines whose links are of different lengths. Moreover, polygonal lines with equal-length links provide with better approximation of the curvature, normal and tangent vectors. Suppose we have started from an initial polygonal line whose vertices are not equally spaced and evolve the line according to the scheme

$$P_i^{(k+1)} = P_i^{(k)} + \varepsilon^{(k)}\, F_i^{(k)}\, \mathbf{n}_i^{(k)}. \qquad (13)$$

To achieve the uniform distribution of vertices we modify (13) by adding a tangential speed and arrive at

$$P_i^{(k+1)} = P_i^{(k)} + \varepsilon^{(k)} \left(F_i^{(k)}\, \mathbf{n}_i^{(k)} + G_i^{(k)}\, \mathbf{t}_i^{(k)} \right),$$

where $\mathbf{t} = \mathbf{n}^{\perp}$ is the unit tangent vector. We set

$$G_i^{(k)} = e^{-ct} \left[d_i^{(k)} - d_{i-1}^{(k)} \right], \qquad (14)$$

where $d_i^{(k)}$ is the distance between two neighboring vertices $P_i^{(k)}$ and $P_{i+1}^{(k)}$, c is a positive constant. From a mechanical point of view this tangent speed term resembles inserting springs between any two neighboring vertices. Adding the speed component (14) does not affect the shape of the limit curve $\{P_i^{(\infty)}\}$ and gives almost uniform distribution of its vertices.

Another numerical trick we use to speed up the convergence consists of variation of the number of the vertices of the evolving polygonal curve. We start from an initial polygonal curve consisting only few links. Therefore, at the beginning of the evolution we can keep the step-size parameter ε to be not small. We insert new vertices between old ones as the evolution approaches to its limit shape. It resembles a subdivision technique.

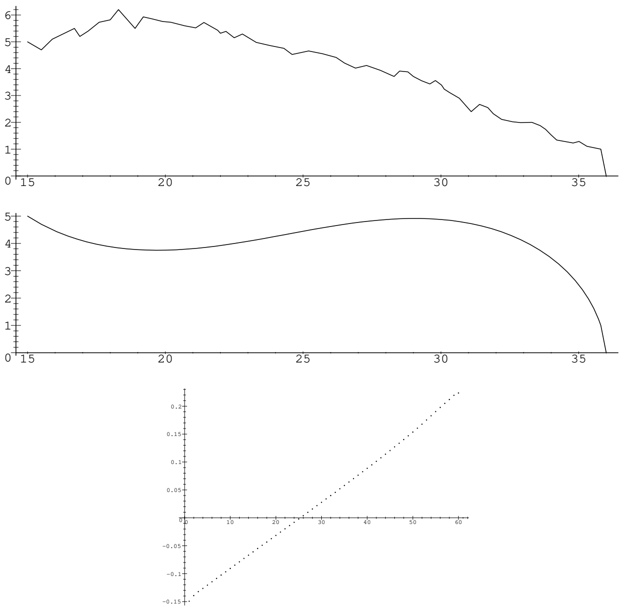

Figure 6. Modeling of wooden splines with curve evolutions. Top: An initial curve. Middle: A wooden spline obtained as the limit of a curve evolution starting from the initial curve. Bottom: The graph of the curvature of the spline.

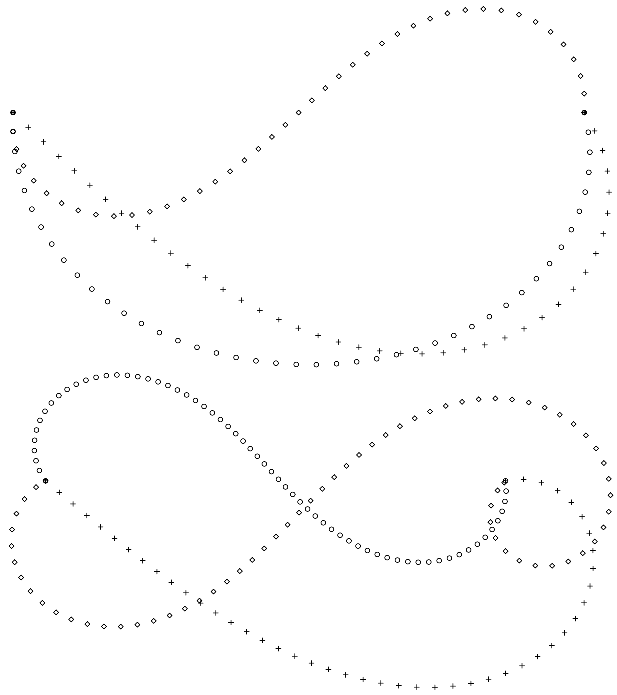

Figure 7. Approximation of wooden splines (top image) and mechanical splines (bottom image) by polygonal curves obtained via curve evolutions. Curvature-curvature boundary conditions: the vertices are marked by crosses. Curvature-tangent boundary conditions: the vertices are marked by circles. Tangent-tangent boundary conditions: the vertices are marked by diamonds.

Fig. 7 shows limit polygonal shapes approximating mechanical (top image) and wooden (bottom image) splines subject to various boundary conditions.

Limitations of the proposed approach

The method proposed in this paper has evident limitations. Below we consider a variety of situations when our approach in its present form can not be applied successfully.

Ill-posed problems. It is well known that difference between the tangent directions of any two points of a mechanical spline does not exceed π (see, for example, [4]). Thus, if we choose the tangent directions θ_A and θ_B at the end-points A and B such that

$$|\,\theta_A - \theta_B| > \pi,$$

then evolution (1), (6) does not converge.

Another ill-posed problem arises when we prescribe boundary curvatures for evolution (1), (6). In our numerical experiments we often observed so-called spiral behavior of the evolving curve. Fig. 8 demonstrates spiral behavior of a curve evolving by (1), (6). At the left end-point the curvature is equal to zero and at the right end-point the curvature is equal to one. This can be explained as follows. Let us construct a curve γ_n passing through two given end-points A and B and satisfying the curvature boundary at the end-points

$$k_A = 1, \quad k_B = 0$$

such that

$$\int_{\gamma_n} k^2\,ds \longrightarrow 0 \quad \text{as} \quad n \to \infty.$$

We compose γ_n from a wooden spline and a straight segment such that the curvature of γ_n has the profile demonstrated at the left image of Fig. 9. We always can do it because the rotations about A and B do not change the curvature boundary conditions (see the middle and right images of Fig. 9). It remains to note that

$$\int_{\gamma_n} k^2\,ds = \int_0^{1/n} (1-ns)^2 ds = \frac{1}{3n} \longrightarrow 0 \quad \text{as} \quad n \to \infty.$$

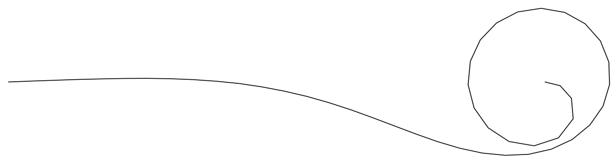

Figure 8.

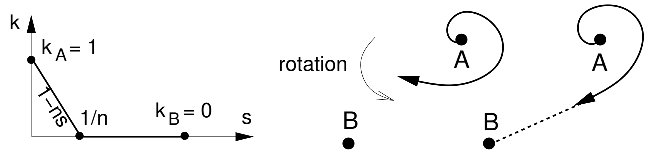

Figure 9.

Thus, a curve driven by (1), (6) and satisfying given point-curvature boundary conditions may develop the spiral behavior like the Cornu spiral has (see Fig. 10).

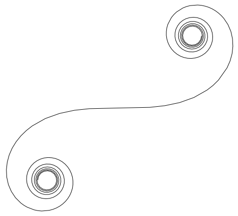

Figure 10.

High-order curvature derivatives. Our approach doesn't work satisfactory to construct curves minimizing integrals containing curvature derivatives. For example, modeling *minimum curvature variation curves* [11] which minimize the energy

$$\frac{1}{2}\int\left(\frac{dk}{ds}\right)^2 ds \longrightarrow \min \tag{15}$$

can be reduced to (1) with

$$F = k'''' + k^2k'' - \frac{5}{2}k\,k'^2.$$

Numerical implementation of this flow is extremely difficult because speed F depends on the fourth derivative of the curvature. Various numerical approaches were proposed to cope with high-order curvature derivatives. See, for example, [11] for minimizing (15) and [1] for design discrete elastica curves.

Non-smooth speed functions. Another obstacle to apply our approach appears when the speed function F is not smooth. For example, suppose we want to join two given end-points with prescribed end-directions at them by a curve minimizing the energy

$$\int |k|^q\,ds \longrightarrow \min, \tag{16}$$

where k is the curvature and q is a given positive constant.

This energy arises, for example, in computational fluid dynamics [5, Chapter 8].

Another possible area where (16) can appear is analysis of human motions. Numerous studies of plane point-to-point hand movements have shown that the movement velocity is related to the radius of curvature of the movement trajectory by a power law with an exponent of $2/3$

$$v = \mathrm{Const}\,k^{-2/3}.$$

See, for example [10, 15], and references therein. Consider a fastest possible plane point-to-point movement. The movement trajectory minimizes (16) with $q = 2/3$.

For $q < 1$ the gradient descent flow for (16) is given by (1) with singular speed F and our method in its present form is not applicable.

To cope with (16) the following simple and elegant approach proposed in [8] for modeling of mechanical splines and elastica can be used. Let $A = (x_A, y_A)$ and $B = (x_B, y_B)$ be two given end-points with prescribed end-directions θ_A and θ_B at them. Here θ is the angle between the curve tangent and the x axis.

Consider a curve passing through the end-points A and B, having prescribed end-directions θ_A and θ_B at the end-points, and minimizing (16). We assume that the curvature of the curve has a fixed sign. We have two constrains

$$\int_{\theta_A}^{\theta_B} \frac{\cos\theta}{k}\,d\theta = x_B - x_A, \quad \int_{\theta_A}^{\theta_B} \frac{\sin\theta}{k}\,d\theta = y_B - y_A. \tag{17}$$

Since $k\,ds = d\theta$, then the Euler equation of the curve minimizing (16) and satisfying the above constrains has the form

$$\frac{d}{dk}\left(k^{q-1} + \frac{1}{k}(\lambda_1\cos\theta + \lambda_2\sin\theta)\right) = 0,$$

where λ_1 and λ_2 are Lagrange multipliers. Therefore,

$$k^q = \lambda\cos(\theta - \theta_0),$$

where the constants λ and θ_0 can be found from (17) by integration.

Conclusion

The paper develops a numerical approach to design nonlinear splines as limit shapes of polygonal curve evolutions.

The approach is tested by modeling wooden and mechanical splines subject to various boundary conditions. Evolutions of polygons for purposes of multiscale shape analysis are also considered. We also demonstrate that out approach is useful to approximate geodesics in two-dimensional Riemannian spaces.

Appendix A

Variation of length and geodesic curvature. For the curve tangent and normal vectors

$$\mathbf{t}(s) = \mathbf{r}'(s), \quad \mathbf{n}(s) = \mathbf{t}(s)^{\perp}.$$

the Frenet formulas give

$$\mathbf{t}'(s) = k\,\mathbf{n}, \quad \mathbf{n}'(s) = -k\,\mathbf{t},$$

where $k(s)$ is the curvature and the derivatives are taken with respect to arc length s.

Consider a small deformation of the curve along the curve normals:

$$\mathbf{r}_{\text{new}}(s) = \mathbf{r}(s) + \varepsilon h(s)\mathbf{n}(s),$$

where ε is small, $h(s)$ is smooth. We have

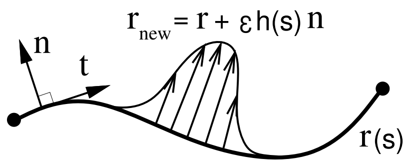

Figure 11.

$$\mathbf{r}'_{\text{new}} = \mathbf{t} + \varepsilon(h'\mathbf{n} - h\,k\,\mathbf{t}),$$

$$ds_{\text{new}} = \sqrt{\mathbf{r}'_{\text{new}} \cdot \mathbf{r}'_{\text{new}}}\,ds = \left[1 - \varepsilon hk + O(\varepsilon^2)\right] ds$$

and, therefore,

$$\int ds_{\text{new}} = \int ds - \varepsilon \int hk\,ds + O(\varepsilon^2).$$

If the plane is equipped with a conformal Riemann metric

$$dl = g(x,y)\sqrt{dx^2 + dy^2}, \tag{18}$$

with $g(x,y) > 0$, then

$$g_{\text{new}} = g(\mathbf{r}_{\text{new}}) = g + \varepsilon h\,\nabla g \cdot \mathbf{n} + O(\varepsilon^2)$$

and

$$\int g_{\text{new}}\,ds_{\text{new}} = \int g\,ds + \varepsilon \int h(\nabla g \cdot \mathbf{n} - gk)\,ds + O(\varepsilon^2).$$

Thus the steepest decent flow for the length functional

$$\int dl = \int g\,ds$$

is given by the flow

$$\frac{\partial \mathcal{C}(p,t)}{\partial t} = F\,\mathbf{n} \tag{19}$$

with

$$F = gk - \nabla g \cdot \mathbf{n}.$$

For the Euclidean plane $g \equiv 0$ and $F = k$. The quantity

$$gk - \nabla g \cdot \mathbf{n}$$

is called the *geodesic curvature* associated with Riemannian metric (18) and the *geodesics* are the curves of zero geodesic curvature.

Example: Poincaré metric. Consider the upper half plane $\{y > 0\}$ with the so-called Poincaré metric

$$dl^2 = \frac{dx^2 + dy^2}{y^2}, \quad g(x,y) = \frac{1}{y}.$$

We have along the geodesics

$$\frac{k}{y} - \nabla \frac{1}{y} \cdot \mathbf{n} = 0. \tag{20}$$

Since $\mathbf{n} = (-y', x')$, one can rewrite (20) as follows

$$x' = -ky. \tag{21}$$

Recall that

$$x' = \cos\theta, \quad y' = \sin\theta, \quad k = \theta',$$

where $\theta(s)$ is the angle between the tangent at $(x(s), y(s))$ and the positive direction of the x-axis. Now differentiating the left and right sides of (21) with respect to arc length s gives

$$\begin{aligned} x'' &= (\cos\theta)' = -\theta'\sin\theta = -k\sin\theta \\ -(ky)' &= -k'y - ky' = -k'y - k\sin\theta. \end{aligned}$$

Thus $k'y = 0$ along the geodesics and it follows $k' = 0$. The equation $k' = 0$ describes the circles and straight lines. For a straight line (21) gives $x' = 0$ and, hence, the line is vertical. For a circle

$$x = A + R\cos\theta, \quad y = B + R\sin\theta$$

equation (21) gives

$$\begin{aligned} x' &= \frac{dx}{d\theta}\,\theta' = -R\sin\theta/R = -\sin\theta \\ ky &= (B + R\sin\theta)/R = \sin\theta + B/R. \end{aligned}$$

Hence $B/R = 0$ and the circle is centered on the x-axis.

Thus we showed that the geodesics in the upper half plane equipped with the Poincaré metric are the vertical lines and semi-circles centered on the x-axis.

Variation of curvature. In our derivation of the variation of curvature we follow [12]. We have

$$\mathbf{t}_{\rm new} = \frac{d\mathbf{r}_{\rm new}}{ds_{\rm new}} = \frac{d\mathbf{r}_{\rm new}}{ds}\frac{ds}{ds_{\rm new}} = \mathbf{t} + \varepsilon h'\mathbf{n} + O(\varepsilon^2),$$

$$\mathbf{n}_{\rm new} = \mathbf{n} - \varepsilon h'\mathbf{t} + O(\varepsilon^2),$$

$$k_{\rm new}\mathbf{n}_{\rm new} = \frac{d\mathbf{t}_{\rm new}}{ds_{\rm new}} =$$

$$= \frac{d\mathbf{t}_{\rm new}}{ds}\frac{ds}{ds_{\rm new}} = \frac{k\mathbf{n} + \varepsilon h''\mathbf{n} - \varepsilon h'k\mathbf{t} + O(\varepsilon^2)}{1 - \varepsilon hk + O(\varepsilon^2)}$$

$$= (k + \varepsilon h'' + \varepsilon hk^2)\mathbf{n} - \varepsilon h'k\mathbf{t} + O(\varepsilon^2) =$$

$$= (k + \varepsilon h'' + \varepsilon hk^2)(\mathbf{n}_{\rm new} + \varepsilon h'\mathbf{t}) - \varepsilon h'k\mathbf{t} + O(\varepsilon^2) =$$

$$= (k + \varepsilon h'' + \varepsilon hk^2)\mathbf{n}_{\rm new} + O(\varepsilon^2).$$

Thus

$$k_{\rm new} = k + \varepsilon\left(h'' + hk^2\right) + O(\varepsilon^2).$$

Thus the curvature of the curve evolving according to (19) satisfies the following partial differential equation

$$\frac{\partial k}{\partial t} = F'' + Fk^2.$$

For the mechanical splines integrating by parts yields

$$\frac{1}{2}\int k_{\rm new}^2\, ds_{\rm new} = \frac{1}{2}\int k^2\, ds + \varepsilon\int\left(k'' + \frac{k^3}{2}\right)h\, ds + O(\varepsilon^2).$$

Thus, along the mechanical splines we have

$$k'' + \frac{k^3}{2} = 0.$$

Evolution of the area and perimeter of a closed curve. For a closed curve driven by flow (19) one has

$$\frac{d}{dt}L(t) = -\int Fk\, ds, \qquad \frac{d}{dt}A(t) = -\int F\, ds.$$

For example, for the flow with

$$F = -k'' \tag{22}$$

we have

$$\frac{d}{dt}L(t) = \int k''k\, ds = -\int k'^2 ds,$$
$$\frac{d}{dt}A(t) = \int k'' ds = 0.$$

Thus the flow preserves the area enclosed by the evolving curve and reduces the perimeter of the curve.

Numerical experiments show that a closed curve driven by (19), (22) converges to a circle. However, as far as we know, a rigorous proof remains an open question (see [14]).

References

[1] A. M. Bruckstein, R. J. Holt, and A. N. Netravali. Discrete elastica. In *Discrete Geometry for Computer Imagery, Lecture Notes in Computer Science 1176*, pages 59–72, Lyon, France, November 1996.

[2] A. M. Bruckstein, G. Sapiro, and D. Shaked. Evolution of planar polygons. *Int. J. Pattern Recogn. Artif. Intell.*, 19(6):991–1014, 1995.

[3] A. M. Bruckstein and D. Shaked. On projective invariant smoothing and evolution of planar curves and polygons. *J. Math. Imag. Vision*, 7:225–240, 1997.

[4] D. Coope, I. Curve interpolation with nonlinear spiral splines. *IMA Journal of Numerical Analysis*, 13:327–341, 1992.

[5] A. Friedman. *Mathematics in Industrial Problems, Part 7*. IMA Volumes in Mathematics and its Applications, Vol. 67, Springer, 1995.

[6] B. K. P. Horn. The curve of least energy. *ACM Trans. on Math. Software*, 9:441–460, 1983.

[7] J. Hoschek and D. Lasser. *Fundamentals of Computer Aided Geometric Design*. A K Peters, Ltd., 1993.

[8] M. Kallay. Plane curves of minimal energy. *ACM Trans. on Math. Software*, 12:219–222, 1986.

[9] B. B. Kimia, A. Tannenbaum, and S. W. Zucker. Shapes, shocks, and deformations: The components of two-dimensional shape and the reaction-diffusion space. *Int. J. of Computer Vision*, 15:189–224, 1995.

[10] M. L. Latash. *Control of Human Movement*. Human Kinetics Publishers, 1993.

[11] H. P. Moreton. *Minimum Curvature Variation Curves, Networks, and Surfaces for Fair Free-Form Shape Design*. PhD thesis, University of California at Berkeley, 1992.

[12] D. Mumford. Elastica and computer vision. In C. L. Bajaj, editor, *Algebraic Geometry and its Applications*, pages 491–506, Springer, 1994.

[13] M. Nitzberg, D. Mumford, and T. Shiota. *Filtering, Segmentation and Depth, Lecture Notes in Computer Science, Vol. 662*. Springer, 1993.

[14] A. Polden. *Curves and Surfaces of Least Total Curvature and Fourth-Order Flows*. PhD thesis, University of Tubingen, Dept. of Mathematics, 1996.

[15] F. E. Pollick and G. Sapiro. Constant affine velocity predicts the 1/3 power law of drawing and planar motion perception. *Vision Research*, 37:347–353, 1997.

[16] G. Sapiro and A. Tannenbaum. Area and length preserving geometric invariant scale-spaces. *IEEE Trans. PAMI*, 17(1):67–72, 1995.

[17] J. A. Sethian. *Level Set Methods*. Cambridge Univ. Press, 1996.

[18] J. E. Taylor. Surface motion due to crystalline surface energy gradient flows. In *Elliptic and Parabolic Methods in Geometry*, pages 145–162. A K Peters, Ltd, 1993.

[19] J. Weickert. *Anisotropic Diffusion in Image Processing*. B. G. Teubner, Stuttgart, 1998.